energy&fuels

pubs.acs.org/EF Article

Probing Aggregation Tendencies in Asphaltenes by Gel Permeation Chromatography. Part 1: Online Inductively Coupled Plasma Mass Spectrometry and Offline Fourier Transform Ion Cyclotron Resonance Mass Spectrometry

Jonathan C. Putman, Rémi Moulian, Caroline Barrère-Mangote, Ryan P. Rodgers, Brice Bouyssiere,* Pierre Giusti, and Alan G. Marshall*

Cite This: *Energy Fuels* 2020, 34, 8308−8315 Read Online

ACCESS | Metrics & More | Article Recommendations | Supporting Information

ABSTRACT: This study probes the nanoaggregation behavior of asphaltenes by gel permeation chromatography (GPC). Compounds containing sulfur, vanadium, and nickel were monitored online with elemental detection by inductively coupled plasma mass spectrometry (ICP-MS), and four fractions that vary in nanoaggregation state were analyzed by positive atmospheric pressure photoionization 9.4 T Fourier transform ion cyclotron resonance mass spectrometry ((+)APPI FT-ICR MS). We also highlight some of the challenges associated with the analysis of asphaltene fractions by direct infusion. Nanoaggregate size and monomer ion yield were inversely correlated. The extremely low ionization efficiency for the largest aggregate GPC fractions collected from the asphaltenes limited their characterization to only a few of the most abundant heteroatom classes. However, for all of the characterizable heteroatom classes, aggregation closely correlated with increased relative abundance of larger, more aliphatic compounds. These observations agree with results from the parent whole crude oil, suggesting that the interactions among the more alkylated compounds in asphaltenes may be a major contributor to asphaltene nanoaggregation.

INTRODUCTION

Asphaltenes are one of the most complex and problematic components of petroleum crude oils. Across[1] the entire production chain, asphaltenes pose potential complications.[2] Upstream, on the oil recovery side, asphaltene deposits can block pipelines, often requiring production shutdowns to remedy, resulting in massive losses. Downstream, on the upgrading and refining side, crude oils with high asphaltene concentrations typically have lower yields and higher maintenance costs. Defined purely on the basis of insolubility in an *n*-alkane solution (typically *n*-pentane or *n*-heptane), asphaltenes are not a well-defined (or well-understood) chemical compound class.[3] Compared to their parent crude oils, asphaltenes are typically more aromatic with greater heteroatom content.[4−6] Thus, historically it has long been hypothesized that $\pi-\pi$ stacking and hydrogen bonding between polar compounds drive asphaltene nanoaggregation, which leads to precipitation and eventual deposition. However, asphaltenes are extremely difficult to analyze due to their tendency to aggregate, resulting in very poor ionization efficiency in mass spectrometry analysis.

Linking molecular structure to aggregation potential requires detailed molecular level information. On a bulk scale, asphaltenes are more aromatic and contain more polar compounds than their parent crude oils. However, recent works have started to illuminate the importance of wax-like interactions between more aliphatic compounds that may contribute to asphaltene aggregation. Unstable asphaltenes have also been shown to have higher binding capacities for alkanes and waxes.[7] Berrueco et al. observed a correlation between decreases in fluorescence intensity and UV absorbance in the largest, excluded molecular weight regime of GPC fractions from asphaltenes, petroleum pitch, and coal-derived materials.[8−10] They hypothesized that compounds in the largest, excluded GPC peak may be larger and more aliphatic.[10] Characterization by Fourier transform ion cyclotron resonance mass spectrometry (FT-ICR-MS) for GPC aggregate fractions collected from a typical atmospheric residue revealed a surprisingly strong correlation between nanoaggregation potential and decreased aromaticity.[11] Large, very aliphatic compounds with extremely low ionization efficiencies comprised the largest, most aggregated fractions. Similar observations have been made in several recent works that have reinforced the correlation between alkylation and decreased GPC elution times.[12−15] Interfacially active asphaltenes (IAA) refer to the subfraction (~2%) of the whole asphaltenes that adsorbs at the surface of water droplets. Characterization of the IAA by electrospray ionization mass spectrometry (ESI-MS) and ^{1}H and ^{13}C nuclear magnetic resonance (NMR) spectroscopy revealed that the interfacially active species have a higher molecular weight distribution. The

Received: May 13, 2020
Revised: June 8, 2020
Published: June 8, 2020

https://dx.doi.org/10.1021/acs.energyfuels.0c01522
Energy Fuels 2020, 34, 8308−8315

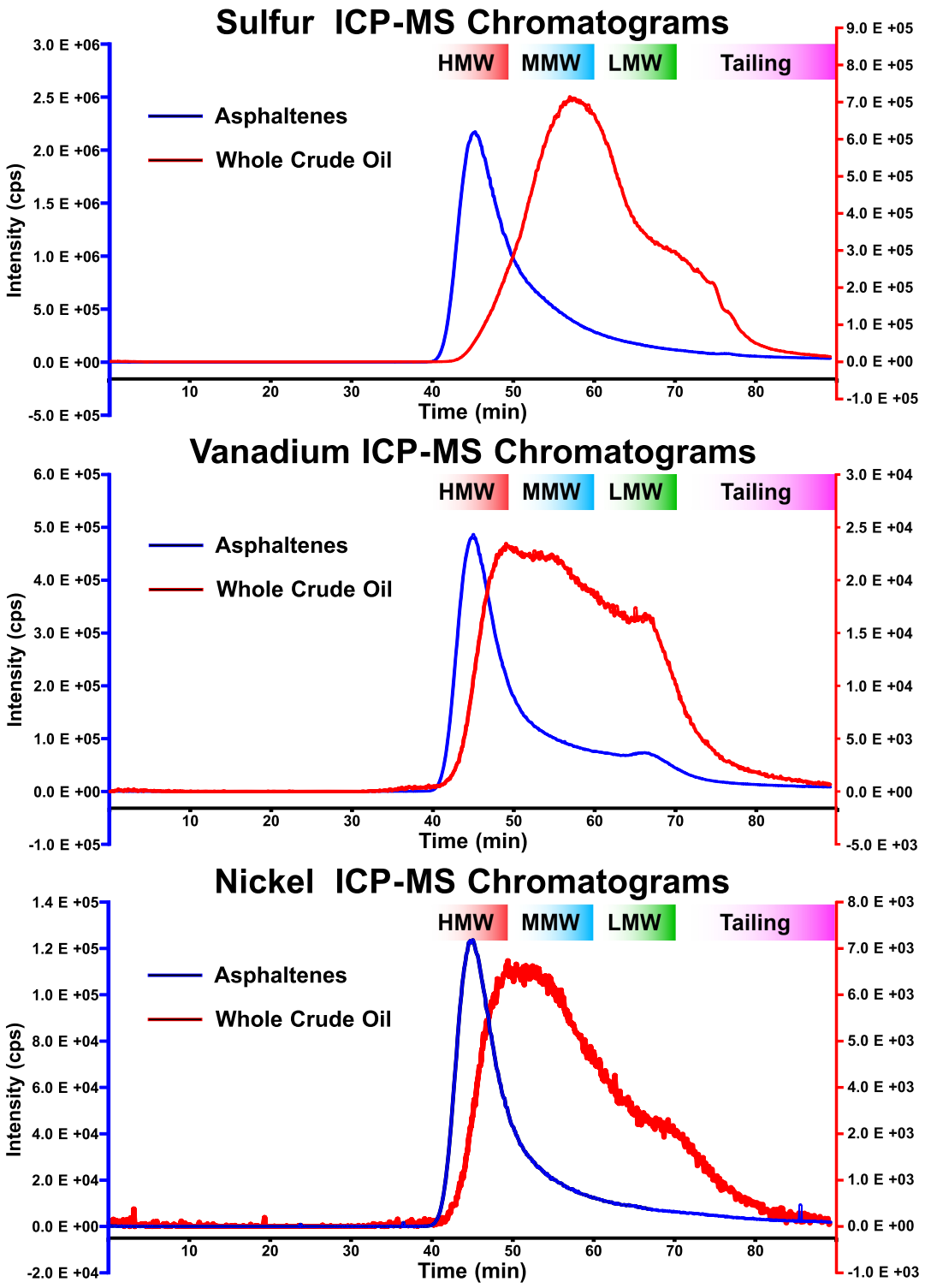

Figure 1. Sulfur (top), vanadium (middle), and nickel (bottom) GPC ICP mass chromatograms. Intensities for the Petrophase 2017 purified asphaltenes are plotted in blue, and parent whole crude oil's intensities are in red. High, medium, and low molecular weight (HMW, MMW, and LMW) and tailing fraction elution ranges are indicated at the top.

IAA was also less aromatic (more aliphatic) on average and was enriched in sulfoxides relative to the whole asphaltenes.[12] Guricza and Schrader also observed similar trends and reported a GPC separation based on both mass and H/C ratio. Compounds with long aliphatic side chains on an aromatic core eluted first, and later-eluting species were primarily condensed polyaromatics with shorter side chains.[16] Works by Panda et al.[14] and Alawani et al.[15] also reported GPC elution based primarily on the degree of alkylation (i.e., more alkylated compounds eluted earliest).

Trace metals present in crude oils also complicate refinery processes by potentially deactivating hydrotreatment and hydrocracking catalysts. Vanadium, nickel, and iron are typically the most abundant metals found in petroleum

https://dx.doi.org/10.1021/acs.energyfuels.0c01522
Energy Fuels 2020, 34, 8308−8315

products. Structurally, these metals are incorporated into heterocyclic macrocycles with four modified pyrrole subunits, known as porphyrins.[17,18] The forces driving asphaltene aggregation are not well understood: although metal-containing petroporphyrins are greatly enriched in precipitated asphaltenes, the nature of their involvement is unknown.[19] To probe the forces driving asphaltene aggregation in a laboratory, gel permeation chromatography (GPC) acts as a proxy for real-world aggregation. However, it is not entirely clear how well on-column nanoaggregation mimics that of asphaltene aggregation in the field.

Inductively coupled plasma mass spectrometry (ICP-MS) coupled with GPC yields quantitative chromatograms, commonly called size distributions or size profiles, for individual elements. For porphyrinic metals like vanadium and nickel, GPC chromatograms generally yield trimodal/multimodal aggregate size profiles sufficiently unique to act as "fingerprints" for petroleum samples.[20,21] The aggregate size profiles also help determine the cut points between GPC aggregate fractions. Significant effort in recent years has been made to understand the importance of GPC aggregate size distributions regarding specific refinery problems. GPC size profiles have been determined for saturates, aromatics, resins, and asphaltenes fractions,[21,22] distillation cuts,[20] and isolated interfacial material.[23] Ideally, analytes should not interact with the GPC stationary phase at all, and elution should be dictated entirely by hydrodynamic volume.[24] Completely eliminating potential surface effects during GPC separations is difficult, if not impossible,[25,26] and mobile phase and column conditions should be chosen to ensure that hydrodynamic volume is the dominant retention mechanism.[10] Even so, caution should be taken not to infer too much from GPC results on their own. For that reason, results presented here will discuss aggregation tendencies observed during GPC separations. In this way, we hope to probe the relationship between the forces driving on-column aggregation and asphaltene nanoaggregation.

Four GPC fractions corresponding to various aggregate sizes were collected from an Arabian heavy crude oil and its corresponding purified asphaltenes for further analysis by 9.4 T Fourier transform ion cyclotron resonance mass spectrometry (FT-ICR-MS). For petroleum product and complex mixtures, differences in ionization efficiency and aggregation tendency between compounds result in the preferential detection of the most easily ionized species. Although ionization bias can be partially overcome by chromatographic separations,[27,28] the choice of ionization method is still critical. Here, we chose positive-ion atmospheric pressure photoionization ((+)APPI), which is believed to be the most suitable method for characterization of asphaltenes.[29−31] Although APPI is well known to preferentially ionize aromatic compounds, ionization is more uniform than electrospray.[29,32] This work is the first part of a two-part study investigating the molecular composition of the PetroPhase 2017 asphaltene sample across a GPC elution profile. Here, we focus on the results from offline fraction collection and direct infusion and highlight some of the challenges we faced with that approach. In part 2, we shall examine the benefits of coupling the GPC method with online detection by 21T FT-ICR-MS, which reveals a more comprehensive molecular characterization.

EXPERIMENTAL METHODS

Instrumentation and Materials. An AKTA*purifier* liquid chromatography system equipped with a UV-900 multiwavelength UV absorbance detector and a Frac-950 fraction collector (GE Healthcare Bio-Sciences, Pittsburgh, PA, USA) was used to perform the GPC separation. As previously described, three Shodex preparative GPC columns were connected in series (KF-2004, KF-2002.5, and KF-2001) (Showa Denko America, Inc., New York, NY, USA).[11] The flow rate was set to 3 mL/min with 100% ACS reagent-grade xylene (Scharlab, S.L., Gato Pérez, Barcelona, Spain). Most of the eluent was directed to a fraction collector by a postcolumn split, and the low-flow outlet from the splitter (~40 μL/min) was diverted to an ICP-MW instrument for elemental detection (Thermo Scientific Element XRsector field ICP-HRMS). ICP experimental conditions have been described extensively in previous works.[11,20,21,33,34]

A custom-built adapter was used to interface the APPI source (ThermoFisher Scientific, San Jose, CA, USA) with the front stage of a custom-built 9.4 T FT-ICR mass spectrometer.[29,35−37] Samples were analyzed by positive APPI with the source set to a vaporization temperature of 350 °C. To avoid sample oxidation, N_2 was used for the sheath gas (50 psi) and the auxiliary gas (32 mL/min). Direct infusion experiments of the samples and fractions were performed at a concentration of 100 μg/mL toluene and a flow rate of 50 μL/min. Analysis of each sample consisted of the coaddition of 100 time-domain transients (each with a 6 s acquisition period) followed by Hanning apodization, Fourier transformation with one zero fill, and broad-band phase correction.[38] The resulting absorption-mode FT-ICR mass spectra had a resolving power greater than 1 100 000 at m/z 500. Predator Analysis and PetroOrg were used to perform calibration and data processing.[36,39]

Purified Asphaltenes. Asphaltenes were isolated from an Arabian heavy crude oil provided by Total according to the standard ASTM D6560-12 method.[40] Once isolated, the asphaltenes were further purified to remove occluded material. Depending on the sample, occluded material can account for as much as 50 wt % of asphaltenes.[41,42] Purification to remove occluded material was performed by four iterations of maceration followed by Soxhlet extraction with clean n-C_7 for 5 h (20 h total) as previously reported.[43] The purified asphaltenes are also referred to as the PetroPhase 2017 asphaltene sample, as they were obtained as part of an international collaborative effort to study asphaltenes (Asphaltene 2017; Asphaltene Characterization Interlaboratory Study for PetroPhase 2017. In *Proceedings of the 18th International Conference on Petroleum Phase Behavior and Fouling*, Le Havre, France, June 11−15, 2017).[44]

RESULTS AND DISCUSSION

Aggregate Size Distributions for Sulfur, Vanadium, and Nickel. Online detection by ICP-MS was utilized during the GPC fractionation to monitor ^{32}S, ^{51}V, and ^{58}Ni isotopes. The mass chromatograms in Figure 1 show that compared to the starting whole crude oil, in red, the mass distributions of the asphaltenes, in blue, shift dramatically to a more aggregated (earlier eluting) state. For the asphaltenes more than one-half of the ICP-MS chromatogram area and more than one-half of the total mass recovered elute in the most-aggregated, highest MW GPC fraction. The mass profiles for sulfur (Figure 1a) exhibit pseudo-monomodal distributions, but the whole crude oil profile centers around the medium and low-MW fractions, whereas the mass profile of the asphaltenes is centered in the high-MW aggregate fraction, in accord with the area distributions and mass recoveries shown in Tables 1 and 2. For the asphaltenes, ~70% of the recovered mass eluted in the largest aggregate high-MW fraction, compared to ~7% for the parent crude oil. The poor recovery of ~75% with xylene as the mobile phase prompted a change in mobile phase to tetrahydrofuran (THF). The eluent was visibly yellowish during the first blank THF injection, likely indicating adsorption of asphaltenic material to the stationary phase. As shown in Table S1, the total mass recovery improved to ~93%

https://dx.doi.org/10.1021/acs.energyfuels.0c01522
Energy Fuels 2020, 34, 8308−8315

Table 1. Average and % RSD for the Mass Recovery and Area Distributions from the Arabian Heavy Crude Parent Oil Sample (n = 3)

fraction	mass recovery (%)	^{32}S area (%)	^{51}V area (%)	^{58}Ni area (%)
high MW	7.4 ± 3.1	3.5 ± 0.3	14.2 ± 0.6	15.3 ± 0.6
medium MW	54.3 ± 5.4	43.3 ± 1.2	37.5 ± 0.9	40.4 ± 0.4
low MW	26.1 ± 6.7	30.0 ± 0.7	27.6 ± 0.4	21.1 ± 0.2
tailing	12.3 ± 0.9	15.7 ± 1.1	10.0 ± 1.4	11.9 ± 0.5
total	93.4 ± 5.6	100	100	100

Table 2. Average and % RSD for the Normalized Mass Recovery and Area Distributions from the Purified Asphaltene Sample (Asphaltene 2017) (n = 3)

fraction	mass recovery (%)	^{32}S area (%)	^{51}V area (%)	^{58}Ni area (%)
high MW	69.4 ± 3.2	51.4 ± 3.2	49.8 ± 3.1	56.8 ± 3.2
medium MW	20.0 ± 1.3	24.0 ± 1.5	21.0 ± 1.1	19.4 ± 1.4
low MW	7.6 ± 2.6	7.9 ± 0.5	13.2 ± 0.8	7.5 ± 0.6
tailing	3.0 ± 1.4	5.8 ± 1.0	6.6 ± 0.9	6.6 ± 1.0
total	74.9 ± 5.2	100	100	100

with THF, with the high-MW fraction still accounting for ~70% of that. Unfortunately, multiple attempts to collect and characterize these fractions by direct infusion were unsuccessful for reasons which will be discussed below. The difficulties associated with fraction collection and analysis by direct infusion will also be addressed in a follow-up study that utilizes online detection by 21T FT-ICR-MS to help overcome the limitations faced during this study. The present results focus on characterization of the GPC aggregate fractions collected with xylene as the mobile phase.

Characterization of Aggregate Fractions by FT-ICR-MS. Further characterization of the asphaltene and its GPC aggregate fractions was performed by positive APPI 9.4 T FT-ICR-MS, and Figure 2 shows the heteroatom class distribution for the whole asphaltene and its GPC aggregate fractions. The most abundant heteroatom classes in the whole asphaltene

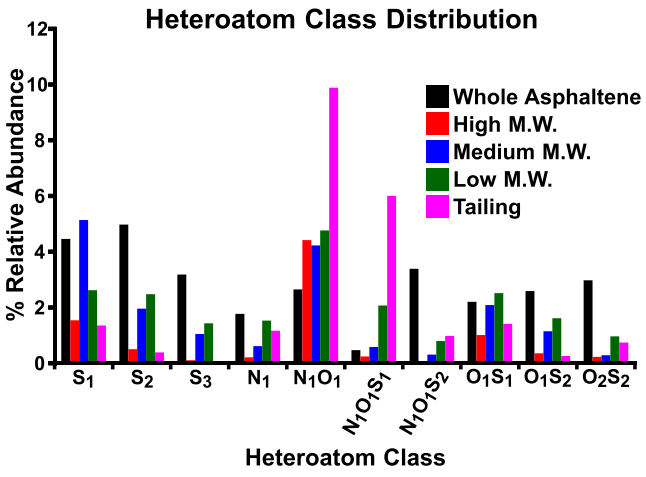

Figure 2. Heteroatom class distributions from (+) APPI 9.4 T FT-ICR mass spectral analysis for the PetroPhase 2017 purified asphaltenes and its corresponding GPC fractions. Heteroatom classes represent the most abundant heteroatom classes for the purified asphaltenes prior to fractionation.

sample were S_x. When measured quantitatively by ICP-MS, more than one-half of the sulfur elutes in the largest aggregate, high-MW fraction. However, the distribution of S_x and O_xS_y heteroatom classes exhibits similar monomodal distributions, with the relative abundance focused around the medium- and low-MW aggregate fractions. The heteroatom class distributions for the parent crude oil and its GPC fractions are provided in the Supporting Information: whereas some of the heteroatom classes shift slightly toward the higher MW aggregate size in the asphaltenes, none of the sulfur-containing heteroatom classes shifted nearly enough to account for the quantitative shift measured by ICP-MS. The relative abundance for heteroatom classes that contain nitrogen increases as aggregation lessens and is most abundant in the smallest aggregate fractions of the asphaltenes.

Figure 3 shows the abundance-weighted average H/C ratios for heteroatom class groups and provides a measure of

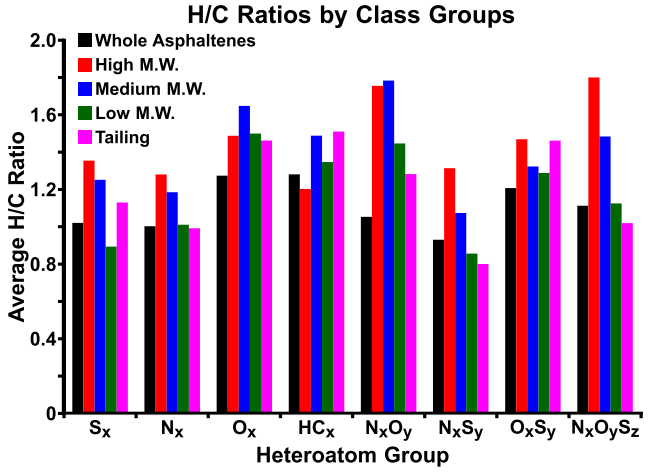

Figure 3. Average H/C ratios for the heteroatom class groups from the purified asphaltenes and its corresponding GPC aggregate fractions.

aromaticity of the asphaltenes and its GPC aggregate fractions. Asphaltenes typically have lower H/C ratios (more aromatic) than their parent crude oils. Because more than 50% of the total mass elutes in the most aggregated high-MW fraction, it would be reasonable to expect the high MW fraction to have the lowest H/C ratios. In fact, we see the opposite trend in the GPC aggregate fractions. For almost all of the heteroatom groups, the high-MW aggregate fraction has the highest H/C ratio, indicating that aggregate size is inversely related to aromaticity. That result is consistent with our previous work on an atmospheric residual sample.[11] Stated concisely, as aggregation increases, there is a general trend toward more aliphatic species. The only two exceptions likely result from our inability to satisfactorily characterize the HC and O_x heteroatom groups. As shown in Figure S1, which is a continuation of Figure 2, the most abundant classes in the GPC aggregate fractions were hydrocarbon (HC) and O_x (O_{1-4}). Together, these classes all sum to less than 5% of the relative abundance in the starting whole asphaltene, but they make up well over one-half of the total signal for all of the GPC aggregate fractions except the tailing fractions. This anomaly, combined with the composition of these heteroatom classes (discussed below and shown in Figure S2), likely indicates contamination in the HC and O_x heteroatom classes. However,

https://dx.doi.org/10.1021/acs.energyfuels.0c01522
Energy Fuels 2020, 34, 8308−8315

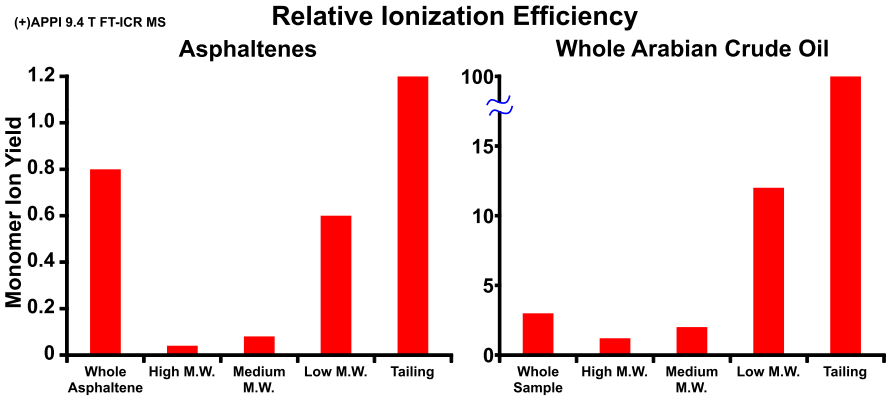

Figure 4. (Right) Monomer ion yields for the Arabian whole crude oil and its fractions. (Left) Monomer ion yields for the purified asphaltenes and its fractions. Ionization efficiencies were calculated from the inverse of the ion accumulation periods used to collect the FT-ICR mass spectra (see text). Those values were then normalized to the tailing fraction from the whole crude oil. Both the whole crude oil and the purified asphaltenes show an inverse relationship between ionization efficiency and aggregate size.

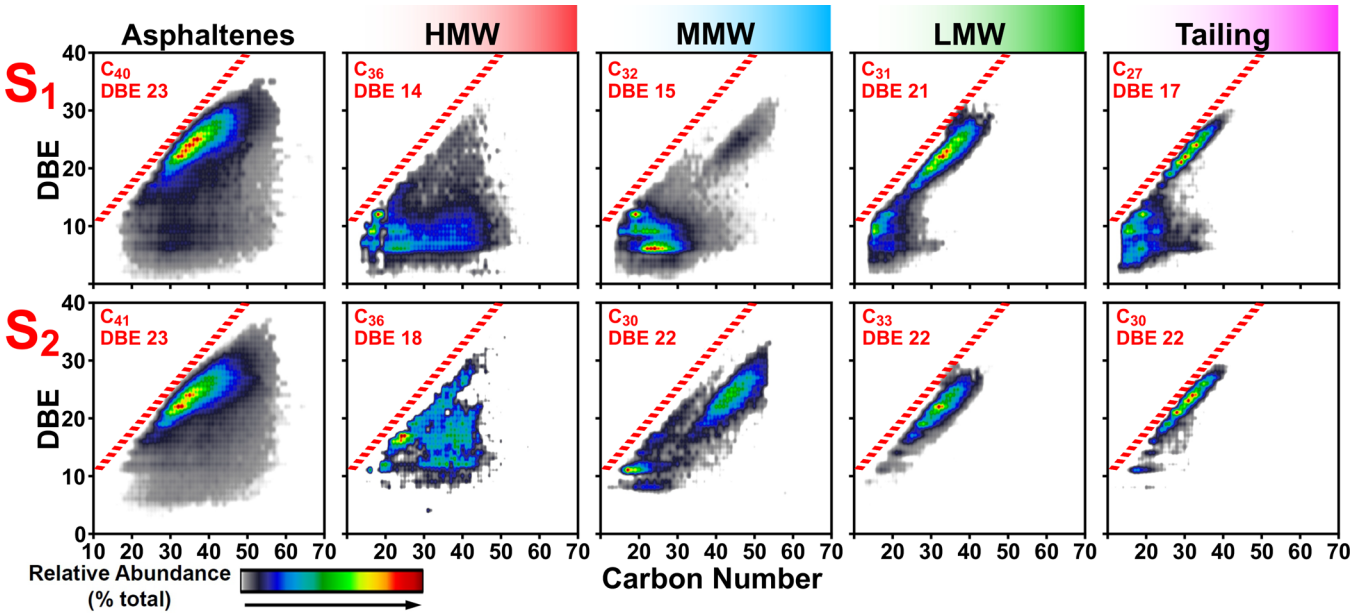

Figure 5. Positive-ion APPI-derived isoabundance-contoured plots of double-bond equivalents vs carbon number for the S_1 class (top) and S_2 class (bottom) for the asphaltenes and its corresponding GPC fractions. Red dashed lines represent the polycyclic aromatic hydrocarbon planar limit.[47,48]

they are included in the Supporting Information in the interest of full transparency.

No apparent trends in the heteroatoms classes or groups explain why the ICP-MS mass profiles (and the mass recovery) shifted to >50% in the largest aggregate GPC fraction of the asphaltenes. However, low ionization efficiencies limited the amount of molecular characterization possible for the GPC aggregate fractions. Asphaltenes are already notoriously difficult to ionize, but the large aggregate GPC fractions were even more challenging. Figure 4 shows the monomer ion yields for the parent crude oil, the asphaltenes, and their GPC aggregate fractions. Calculated from the inverse of the accumulation period required to reach a target number of ions, monomer ion yield provides a qualitative comparison of ionization efficiencies.[27,45] For both the crude oil and the asphaltenes, aggregate size is correlated inversely with monomer ion yield: the largest aggregate fractions ionize least efficiently. The high- and medium-MW aggregate fractions from the asphaltenes required 20−30 s accumulation periods, compared to just a few milliseconds to accumulate the same number of ions in the tailing fraction of the parent crude oil. Such long accumulation periods mean that any chemical contaminants introduced from blowing down large volumes of solvents can completely swamp the sample signal. It took several attempts to sufficiently minimize sources of chemical contamination to obtain useful data. However, there were still chemical contaminant peaks ∼1000× greater in magnitude than the signal from the sample. The high-magnitude contaminant peaks resulted in large fluctuations in the mass error, which made it difficult to identify a Kendrick series[46] to enable calibration. Ultimately, each spectrum had to be broken up into 50−100 Da segments and calibrated separately before the resultant peak lists were recombined and molecular formulas could be assigned reliably. Also, due to the dynamic range limitation of our instrument (∼50 000), characterization was limited to only the most abundant heteroatom classes.

Molecular Composition of GPC Nanoaggregate Fractions from Asphaltenes. Figure 5 shows isoabun-

https://dx.doi.org/10.1021/acs.energyfuels.0c01522
Energy Fuels 2020, 34, 8308−8315

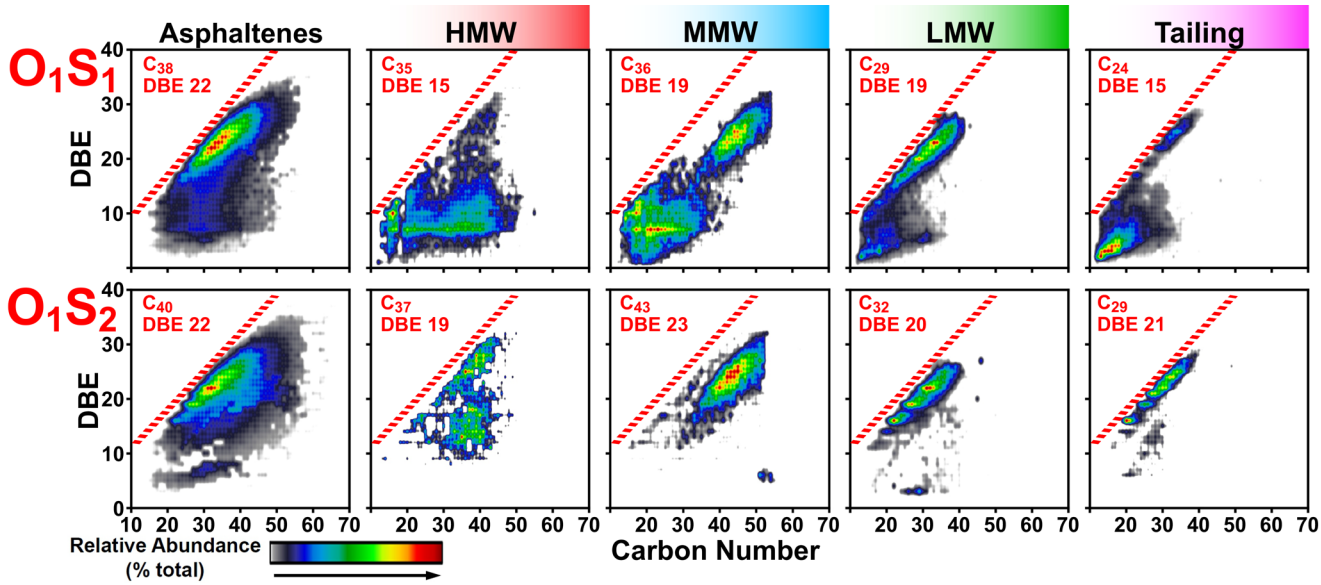

Figure 6. Positive ion APPI-derived isoabundance-contoured plots of double-bond equivalents vs carbon number for the O_1S_1 class (top) and O_1S_2 class (bottom) for the asphaltenes and its corresponding GPC fractions. Red dashed lines represent the polycyclic aromatic hydrocarbon planar limit.

dance-contoured plots of double-bond equivalents (DBE = number of rings plus double bonds to carbon) vs carbon number for the S_1 (top) and S_2 (bottom) heteroatom classes, which had the greatest relative abundance in the asphaltenes prior to fractionation. The abundance-weighted average carbon number and average DBE are displayed in the corner of each plot. On the far left, plots for the whole asphaltenes exhibit a fairly typical compositional range for asphaltenes with distributions out to ~60 carbons, average carbon numbers of ~40−41, and average DBE values of ~23. The red dashed lines represent the polycyclic aromatic hydrocarbon (PAH) planar limit and provide a comparison of aromaticity for the aggregate fractions.[47,48] On the far right, the tailing fraction has a lower average number of carbons than the whole sample and does not contain any species with greater than ~40 carbons. The most abundant hot spots for both classes are highly aromatic and occupy locations very close to the PAH planar limit. The compositional range for the low-MW GPC aggregate fraction is slightly displaced from the PAH planar limit, but both classes still contain highly aromatic species. The medium-MW GPC fraction, shown in the middle of Figure 6, occupies a compositional range even further displaced from the PAH planar limit. Species present with DBE greater than 20 are more alkylated with a distribution from ~40 to 55 carbons. In the lower DBE range, the hot spot at DBE 6 in the S1 heteroatom class corresponds to a benzothiophene core (8 aromatic carbons) and as many as 40 aliphatic carbons are present as alkyl substitutions. Together, the compositional range spanned by the tailing, low-MW, and medium-MW reconstitutes the distribution of the whole asphaltenes fairly well for both heteroatom classes. The largest aggregate, high-MW fraction continues the observed trends, and the distribution is significantly more aliphatic. The high-MW fraction has the lowest average DBE and the greatest average carbon number for both classes. The compositional range corresponds to compounds that are the most aliphatic, and the distribution becomes less aromatic as aggregate size increases. The most abundant species likely have ~2−4 aromatic rings, as nonaromatics ionize very poorly by APPI, and likely contain very long alkyl chains. It is interesting to note that compounds with DBE 6 and 50 carbons are likely entrained material that coprecipitated with the purified asphaltenes, because they should be soluble in heptane on their own. As shown in Figure 6, the same observations discussed above were also made for the O_1S_1 and O_1S_2 heteroatom classes, which were among the most abundant heteroatom classes in the whole asphaltene prior to fractionation. The average composition shifts to larger, more aliphatic compounds as aggregate size increases.

Note that the compositional range spanned by the whole asphaltenes can be more or less reconstructed from those for the fractions for those heteroatom classes. S_x and O_xS_y classes were among the most abundant prior to fractionation; however, as discussed above, HC and O_x accounted for more than one-half of the relative abundance in the asphaltenes fractions. The isoabundance-contoured plots for the HC, O_1, and O_2 heteroatom classes are included in the Supporting Information to highlight the limitations of fraction collection and analysis by direct infusion for difficult to ionize/analyze samples. Compared to the compositional range spanned prior to fractionation, the distributions for the fractions, shown in Figure S2, could not come close to reconstructing that for the whole asphaltenes. Especially for the O_x classes, the only observable features in the composition of the fractions are almost exclusively hot spots that correspond to chemical contaminant peaks.

The heteroatom class distribution and isoabundance-contoured plots for the HC, S_1, S_2, and O_1S_1 heteroatom classes from the whole crude oil and its corresponding GPC aggregate fractions are included in the Supporting Information. The heteroatom class distribution (Figure S3) shows that the most abundant classes for the whole crude oil were HC, S_1, S_2, and O_1S_1. It is difficult to draw meaningful conclusions from the heteroatom class distributions for the corresponding GPC aggregate fractions alone, but the compositions of the HC, S_1, S_2, and O_1S_1 heteroatom classes are shown in Figure S4 (listed from top to bottom). The composition of the whole crude oil

https://dx.doi.org/10.1021/acs.energyfuels.0c01522
Energy Fuels 2020, 34, 8308−8315

is shown at the far left, and the tailing fraction is shown at the far right. As reported previously[11] and as observed in the asphaltene aggregate fractions, the composition becomes increasingly aliphatic as aggregate size increases. The abundance-weighted average carbon number for the medium-MW fraction is more than double that for the tailing fraction for all four classes, and the average DBE is lower for three out of the four classes. For all four heteroatom classes, any compounds with more than ~40 carbons with DBE less than ~10 elute in the medium- or high-MW aggregate fractions. Note that the composition of the largest aggregate, high-MW fraction is actually higher in aromaticity. The compositional range for the S_1 and S_2 heteroatom classes in the high-MW fraction is similar to that for the tailing fraction. Structural differences similar to those reported by Chacon-Patiño et al. (i.e., archipelago vs island) may account for the differences in aggregation potential.[27] However, the compositional range spanned by the HC and O_1S_1 heteroatom classes in the high-MW fraction more closely resembles that for the asphaltene fraction. Those classes exhibit pseudobimodal distributions with part centered close to the PAH limit in the high-DBE region and long, aliphatic, alkyl substitutions observed in the low-DBE region.

CONCLUSIONS

Monomer ion yield and aggregation state were strongly correlated in both the crude oil and the asphaltenes. The monomer ion yields of the two largest aggregate GPC fractions (high MW and medium MW) from the asphaltenes were ~1000 times lower than that of the least aggregated, tailing fraction from the whole crude. Due to the extremely low monomer ion yields in these fractions, analysis was limited to only the most abundant heteroatom classes in the asphaltenes. Note that it is difficult, if not impossible, to determine the extent to which the observed heteroatom classes represent the actual composition of the high- and medium-MW GPC fractions; it is entirely possible that additional heteroatom classes are present but ionize so poorly due to their aggregation state that they are not observed. However, for all of the heteroatom classes that we were able to characterize, both in the whole crude oil and in the purified asphaltenes, we observed a strong correlation between aggregation tendency and more aliphatic compounds. As aggregate size decreased, the composition shifted toward more condensed aromatics. No clear evidence of polar functionalities driving aggregation during the GPC separation was observed. A follow-up study will utilize online GPC with detection by 21 T FT-ICR-MS to overcome the limitations associated with fraction collection and direct infusion experiments.

ASSOCIATED CONTENT

Supporting Information

The Supporting Information is available free of charge at https://pubs.acs.org/doi/10.1021/acs.energyfuels.0c01522.

Average and % RSD for the normalized mass recovery from the purified asphaltene sample with THF as diluent and mobile phase (n = 3); positive-ion APPI-derived isoabundance-contoured plots of double-bond equivalents vs carbon number for the HC, O_1, and O_2 heteroatom classes which were most abundant in the high-MW GPC aggregate fraction; positive-ion APPI-derived isoabundance-contoured plots of double-bond equivalents vs carbon number for the HC, O_1, and O_2 heteroatom classes which were most abundant in the high-MW GPC aggregate fraction; heteroatom class distributions from (+) APPI 9.4 T FT-ICR mass spectral analysis of the whole Arabian crude oil and its corresponding GPC fractions; isoabundance contoured plots of double-bond equivalents vs carbon number derived from (+) APPI analysis of the whole crude oil and its GPC aggregate fractions; zoom insets of two mass segments from the broad-band mass spectra of the purified asphaltene and its GPC fractions; average H/C ratios for the heteroatom class groups from the parent whole crude oil and its corresponding GPC aggregate fractions (PDF)

AUTHOR INFORMATION

Corresponding Authors

Brice Bouyssiere − *International Joint Laboratory−iC2MC: Complex Matrices Molecular Characterization TRTG, BP 27, Harfleur 76700, France; TOTAL Raffinage Chimie TRTG, BP 27, Harfleur 76700, France; Institut des Sciences Analytiques et de Physico-chimie pour l'Environnement et les Materiaux, Universite de Pau et des Pays de l'Adour, E2S UPPA, CNRS, IPREM UMR5254, Pau 64053, France;* orcid.org/0000-0001-5878-6067; Phone: +33(0) 559 407 752; Email: Brice.bouyssiere@univ-pau.fr; Fax: +33(0) 559 407 781

Alan G. Marshall − *National High Magnetic Field Laboratory and Department of Chemistry and Biochemistry, Florida State University, Tallahassee, Florida 32310, United States;* orcid.org/0000-0001-9375-2532; Phone: 850-644-0529; Email: marshall@magnet.fsu.edu; Fax: 850-644-1366

Authors

Jonathan C. Putman − *National High Magnetic Field Laboratory and Department of Chemistry and Biochemistry, Florida State University, Tallahassee, Florida 32310, United States; Exum Instruments, Denver, Colorado 80223, United States*

Rémi Moulian − *International Joint Laboratory−iC2MC: Complex Matrices Molecular Characterization TRTG, BP 27, Harfleur 76700, France; TOTAL Raffinage Chimie TRTG, BP 27, Harfleur 76700, France; Institut des Sciences Analytiques et de Physico-chimie pour l'Environnement et les Materiaux, Universite de Pau et des Pays de l'Adour, E2S UPPA, CNRS, IPREM UMR5254, Pau 64053, France*

Caroline Barrère-Mangote − *International Joint Laboratory−iC2MC: Complex Matrices Molecular Characterization TRTG, BP 27, Harfleur 76700, France; TOTAL Raffinage Chimie TRTG, BP 27, Harfleur 76700, France*

Ryan P. Rodgers − *National High Magnetic Field Laboratory, Department of Chemistry and Biochemistry, and Future Fuels Institute, Florida State University, Tallahassee, Florida 32310, United States; International Joint Laboratory−iC2MC: Complex Matrices Molecular Characterization TRTG, BP 27, Harfleur 76700, France; Institut des Sciences Analytiques et de Physico-chimie pour l'Environnement et les Materiaux, Universite de Pau et des Pays de l'Adour, E2S UPPA, CNRS, IPREM UMR5254, Pau 64053, France;* orcid.org/0000-0003-1302-2850

Pierre Giusti − *International Joint Laboratory−iC2MC: Complex Matrices Molecular Characterization TRTG, BP 27,*

https://dx.doi.org/10.1021/acs.energyfuels.0c01522
Energy Fuels 2020, 34, 8308−8315

Harfleur 76700, France; TOTAL Raffinage Chimie TRTG, BP 27, Harfleur 76700, France; orcid.org/0000-0002-9569-3158

Complete contact information is available at: https://pubs.acs.org/10.1021/acs.energyfuels.0c01522

Notes

The authors declare no competing financial interest.

■ ACKNOWLEDGMENTS

This work was performed at the National High Magnetic Field Laboratory ICR User Facility, which is supported by the National Science Foundation Division of Chemistry through Cooperative Agreements DMR-1157490 and DMR-1644779, the State of Florida, Conseil Régional d'Aquitaine (20071303002PFM), and FEDER (31486/08011464). The authors thank TOTAL for supplying oil samples and Steven M. Rowland for helpful discussions and feedback.

■ REFERENCES

(1) Becker, C. H.; Gillen, K. T. *Anal. Chem.* **1984**, *56* (9), 1671−1674.
(2) Akbarzadeh, K.; Hammami, A.; Kharrat, A.; Zhang, D.; Allenson, S.; Creek, J.; Kabir, S.; Jamaluddin, A.; Marshall, A. G.; Rodgers, R. P.; Mullins, O. C.; Solbakken, T. *Oilfield Rev.* **2007**, *19* (2), 22−43.
(3) Fan, T.; Buckley, J. S. *Energy Fuels* **2002**, *16* (6), 1571−1575.
(4) Miller, J. T.; Fisher, R. B.; Thiyagarajan, P.; Winans, R. E.; Hunt, J. E. *Energy Fuels* **1998**, *12* (6), 1290−1298.
(5) Rogel, E.; Roye, M.; Vien, J.; Miao, T. *Energy Fuels* **2015**, *29* (4), 2143−2152.
(6) Buenrostro-Gonzalez, E.; Groenzin, H.; Lira-Galeana, C.; Mullins, O. C. *Energy Fuels* **2001**, *15* (4), 972−978.
(7) Orea, M.; Ranaudo, M. A.; Lugo, P.; López, L. *Energy Fuels* **2016**, *30* (10), 8098−8113.
(8) Hansen, B. E.; Malmros, O.; Turner, N. R.; Stenby, E. H.; Andersen, S. I. In *Proceedings of Light Metals*, New Orleans, LA, 2001; pp 559−564.
(9) Lazaro, M. J.; Islas, C. A.; Herod, A. A.; Kandiyoti, R. *Energy Fuels* **1999**, *13* (6), 1212−1222.
(10) Berrueco, C.; Venditti, S.; Morgan, T. J.; Álvarez, P.; Millan, M.; Herod, A. A.; Kandiyoti, R. *Energy Fuels* **2008**, *22* (5), 3265−3274.
(11) Putman, J. C.; Gutiérrez Sama, S.; Barrère-Mangote, C.; Rodgers, R. P.; Lobinski, R.; Marshall, A. G.; Bouyssière, B.; Giusti, P. *Energy Fuels* **2018**, *32*, 12198−12204.
(12) Qiao, P.; Harbottle, D.; Tchoukov, P.; Masliyah, J.; Sjoblom, J.; Liu, Q.; Xu, Z. *Energy Fuels* **2017**, *31*, 3330−3337.
(13) Molnárné Guricza, L.; Schrader, W. *Fuel* **2018**, *215*, 631−637.
(14) Panda, S. K.; Alawani, N. A.; Lajami, A. R.; Al-Qunaysi, T. A.; Muller, H. *Fuel* **2019**, *235*, 1420−1426.
(15) Alawani, N. A.; Panda, S. K.; Lajami, A. R.; Al-Qunaysi, T. A.; Muller, H. *Energy Fuels* **2020**, *34*, 5414−5425.
(16) Ghislain, T.; Molnarne Guricza, L.; Schrader, W. *Rapid Commun. Mass Spectrom.* **2017**, *31* (2016), 495−502.
(17) Xu, H.; Que, G.; Yu, D.; Lu, J. *Energy Fuels* **2005**, *19* (6), 517−524.
(18) López, L.; Lo Mónaco, S.; Richardson, M. *Org. Geochem.* **1998**, *29* (1-3), 613−629.
(19) Gascon, G.; Vargas, V.; Feo, L.; Castellano, O.; Castillo, J.; Giusti, P.; Acavedo, S.; Lienemann, C. P.; Bouyssiere, B. *Energy Fuels* **2017**, *31* (8), 7783−7788.
(20) Desprez, A.; Bouyssiere, B.; Arnaudguilhem, C.; Krier, G.; Vernex-Loset, L.; Giusti, P. *Energy Fuels* **2014**, *28*, 3730−3737.
(21) Gutierrez Sama, S.; Desprez, A.; Krier, G.; Lienemann, C.-P.; Barbier, J. J.; Lobinski, R.; Barrere-Mangote, C.; Giusti, P.; Bouyssiere, B. *Energy Fuels* **2016**, *30* (9), 6907−6912.
(22) Cui, Q.; Nakabayashi, K.; Ma, X.; Miyawaki, J.; Al-Mutairi, A.; Marafi, A. M.; Park, J.-I.; Yoon, S.-H.; Mochida, I. *Energy Fuels* **2017**, *31* (7), 6637−6648.
(23) Ligiero, L. M.; Bouriat, P.; Dicharry, C.; Passade-Boupat, N.; Lalli, P. M.; Rodgers, R. P.; Barrère-Mangote, C.; Giusti, P.; Bouyssiere, B. *Energy Fuels* **2017**, *31* (2), 1065−1071.
(24) Lathe, G. H.; Ruthven, C. R. J. *Biochem. J.* **1956**, *62* (4), 665−674.
(25) Sato, S.; Takanohashi, T.; Tanaka, R. *Energy Fuels* **2005**, *19* (5), 1991−1994.
(26) Prokai, L.; Simonsick, W. J., Jr. *Rapid Commun. Mass Spectrom.* **1993**, *7* (9), 853−856.
(27) Chacón-Patiño, M. L.; Rowland, S. M.; Rodgers, R. P. *Energy Fuels* **2018**, *32* (1), 314−328.
(28) Rowland, S. M.; Robbins, W. K.; Corilo, Y. E.; Marshall, A. G.; Rodgers, R. P. *Energy Fuels* **2014**, *28* (8), 5043−5048.
(29) McKenna, A. M.; Marshall, A. G.; Rodgers, R. P. *Energy Fuels* **2013**, *27* (3), 1257−1267.
(30) Itoh, N.; Aoyagi, Y.; Yarita, T. *J. Chromatogr. A* **2006**, *1131* (1−2), 285−288.
(31) Robb, D. B.; Covey, T. R.; Bruins, a. P. *Anal. Chem.* **2000**, *72* (15), 3653−3659.
(32) Andreatta, G.; Bostrom, N.; Mullins, O. C. *Langmuir* **2005**, *21* (7), 2728−2736.
(33) Giusti, P.; Nuevo Ordonez, Y.; Philippe Lienemann, C.; Schaumloffel, D.; Bouyssiere, B.; Lobinski, R. *J. Anal. At. Spectrom.* **2007**, *22* (1), 88−92.
(34) Caumette, G.; Lienemann, C.-P.; Merdrignac, I.; Paucot, H.; Bouyssiere, B.; Lobinski, R. *Talanta* **2009**, *80* (2), 1039−1043.
(35) Kaiser, N. K.; Quinn, J. P.; Blakney, G. T.; Hendrickson, C. L.; Marshall, A. G. *J. Am. Soc. Mass Spectrom.* **2011**, *22* (8), 1343−1351.
(36) Blakney, G. T.; Hendrickson, C. L.; Marshall, A. G. *Int. J. Mass Spectrom.* **2011**, *306* (2−3), 246−252.
(37) Purcell, J. M.; Hendrickson, C. L.; Rodgers, R. P.; Marshall, A. G. b. *Anal. Chem.* **2006**, *78* (16), 5906−5912.
(38) Xian, F.; Hendrickson, C. L.; Blakney, G. T.; Beu, S. C.; Marshall, A. G. *Anal. Chem.* **2010**, *82* (21), 8807−8812.
(39) Corilo, Y. E. *PetroOrg. Software*; Florida State University: Tallahassee, FL,2017.
(40) ASTM D6560. *Standard Test Method for Determination of Asphaltenes (Heptane Insolubles) in Crude Petroleum and Petroleum Products*; ASTM International: West Conshohocken, PA, 2017; www.astm.org.
(41) Derakhshesh, M.; Bergmann, A.; Gray, M. R. *Energy Fuels* **2013**, *27* (4), 1748−1751.
(42) Strausz, O. P.; Torres, M.; Lown, E. M.; Safarik, I.; Murgich, J. *Energy Fuels* **2006**, *20* (5), 2013−2021.
(43) Chacón-Patiño, M. L.; Vesga-Martínez, S. J.; Blanco-Tirado, C.; Orrego-Ruiz, J. A.; Gómez-Escudero, A.; Combariza, M. Y. *Energy Fuels* **2016**, *30* (6), 4550−4561.
(44) Giusti, P.; Bouyssière, B.; Carrier, H.; Afonso, C. *Energy Fuels* **2018**, *32*, 2641.
(45) Chacón-Patiño, M. L.; Rowland, S. M.; Rodgers, R. P. *Energy Fuels* **2017**, *31* (12), 13509−13518.
(46) Hughey, C. A.; Hendrickson, C. L.; Rodgers, R. P.; Marshall, A. G.; Qian, K. *Anal. Chem.* **2001**, *73* (19), 4676−4681.
(47) Hsu, C. S.; Lobodin, V. V.; Rodgers, R. P.; McKenna, A. M.; Marshall, A. G. *Energy Fuels* **2011**, *25* (5), 2174−2178.
(48) Lobodin, V. V.; Marshall, A. G.; Hsu, C. S. *Anal. Chem.* **2012**, *84* (7), 3410−3416.